Membrane Bending Modulus and Adhesion Energy of Wild-Type and Mutant Cells of *Dictyostelium* Lacking Talin or Cortexillins

Rudolf Simson,* Eva Wallraff,# Jan Faix,# Jens Niewöhner,# Günther Gerisch,# and Erich Sackmann*
*Physics Department, Biophysics E22, Technische Universität München, D-85748 Garching, and #Max-Planck-Institut für Biochemie, D-82152 Martinsried, Germany

ABSTRACT We have employed an interferometric technique for the local measurement of bending modulus, membrane tension, and adhesion energy of motile cells adhering to a substrate. Wild-type and mutant cells of *Dictyostelium discoideum* were incubated in a flow chamber. The flow-induced deformation of a cell near its adhesion area was determined by quantitative reflection interference contrast microscopy (RICM) and analyzed in terms of the elastic boundary conditions: equilibrium of tensions and bending moments at the contact line. This technique was employed to quantify changes caused by the lack of talin, a protein that couples the actin network to the plasma membrane, or by the lack of cortexillin I or II, two isoforms of the actin-bundling protein cortexillin. Cells lacking either cortexillin I or II exhibited reduced bending moduli of 95 and 160 k_BT, respectively, as compared to 390 k_BT, obtained for wild-type cells. No significant difference was found for the adhesion energies of wild-type and cortexillin mutant cells. In cells lacking talin, not only a strongly reduced bending modulus of 70 k_BT, but also a low adhesion energy one-fourth of that in wild-type cells was measured.

INTRODUCTION

For an amoeboid cell, the composite plasma membrane, comprising the lipid-protein bilayer and the subjacent actin cortex, controls the shape and motility of a cell as well as its ability to adhere to a solid substrate (Sackmann, 1994). Key parameters are the intrinsic stiffness of the cytoskeleton and its coupling to the lipid-protein bilayer. These parameters reflect the activities of a wide variety of proteins that mediate the cross-linkage and bundling of actin filaments (Sato et al., 1987; Janmey et al., 1990), as well as the binding of these filaments to the protein-lipid bilayer (Horwitz et al., 1986; Isenberg and Goldmann, 1992; Geiger et al., 1995; Jockusch et al., 1995)

In previous studies, the effect of cytoskeletal proteins on the motion of *Dictyostelium discoideum* cells was addressed (Schindl et al., 1995; Weber et al., 1995). Mutants lacking two actin cross-linking proteins, α-actinin and 120-kDa gelation factor, and an actin filament-severing protein, the gelsolin homolog severin, did not differ significantly from wild-type cells in their motility on albumin-coated glass, a substrate of optimal adhesiveness. However, on freshly cleaved mica, a weakly adhesive substrate, the motility of the triple mutants was impeded. This behavior could be attributed to a reduced bending elastic modulus of the composite plasma membrane due to the elimination of actin cross-linking proteins. More recently, an influence of the same actin cross-linking proteins on the viscoelastic properties of a pellet of *Dictyostelium* cells has been shown in a rheological study using a torsion pendulum (Eichinger et al., 1996).

To quantify the influence of actin-binding proteins on the bending elasticity of the cell cortex and the strength of adhesion in single cells, we developed an interferometric technique for measuring bending modulus, membrane tension, and adhesion energy. Adhering cells were exposed to a small hydrodynamic flow. It is impossible to evaluate the flow-induced deformation of the cell envelope as a whole because of its very complex and heterogeneous structure. Locally, however, the shape of the composite cell envelope is in good approximation determined by two elastic boundary conditions: the equilibria of tensions and bending moments. We used reflection interference contrast microscopy (RICM) to determine the flow-induced deformation of the cell contour near the contact area. Analysis of this local deformation in terms of the above boundary conditions yields values for the bending modulus and the adhesion energy, without having to consider global shape changes of the cell.

Viscous shear forces have been successfully used to measure molecular parameters of cell adhesion, such as the kinetics of formation and breakage of receptor-ligand bonds (Evans, 1985; Hammer and Lauffenburger, 1987; Xia et al., 1993; Xiao and Truskey, 1996) or the density of receptors (Alon et al., 1995). Flow chambers have been employed for studying detachment (Gallik et al., 1989; Xia et al., 1994), adhesion (Tissot et al., 1992; Olivier and Truskey, 1993), or rolling of cells (Zhao et al., 1995) on functionalized substrates. In these studies the laminar flow velocity was usually high enough to detach the cells. In the present study the shear forces were kept small to minimize deformation of the cells and to avoid their detachment. The exerted shear forces altered the cell contour near the adhesion area only slightly. The small changes in this area could be detected with high accuracy by using RICM.

Received for publication 13 May 1997 and in final form 26 September 1997.

Address reprint requests to Dr. Rudolf Simson, Technische Universität München, Institut für Biophysik E22, 85748 Garching, Germany. Tel.: ++49-89-2891-2478; Fax: ++49-89-2891-2469; E-mail: rsimson@physik.tu-muenchen.de.

0006-3495/98/01/514/09 $2.00

To determine the influence of specific actin-binding proteins on the intrinsic stiffness of cell-cortex and on cortex-bilayer coupling, we compared mutant cells deficient in cortexillin I, cortexillin II, or talin with wild-type cells. Cortexillins I and II contain the conserved actin-binding sites characteristic of the α-actinin/spectrin superfamily of F-actin cross-linking proteins (Faix et al., 1996). The cortexillins are distinguished from other members of this superfamily by forming parallel dimers through the interaction of a long coiled-coil domain in the C-terminal halves of the subunits. Elimination of either isoform causes slight deficiencies in cytokinesis, resulting in an increased proportion of multinucleated cells. The isoforms cooperate in enabling the cells to divide and in stabilizing the cell shape. Elimination of both cortexillins results in giant, extremely flat multinucleated cells (Faix et al., 1996). The focal adhesion protein talin of vertebrate cells binds to β-integrin (Horwitz et al., 1986) and nucleates actin polymerization at lipid membranes (Kaufmann et al., 1992), thereby playing a key role in coupling the actin cortex to the membrane (Isenberg and Goldmann, 1992; Jockusch et al., 1995; Geiger et al., 1995). *Dictyostelium* cells contain a full-length talin homolog of 269 kDa. Elimination of this protein by targeted gene disruption results in reduced substrate adhesion and in a conditional phagocytosis defect, depending on the adhesiveness of the particle to be taken up (Niewöhner et al., 1997).

Compared to wild-type cells, the cells of all three mutants exhibited markedly reduced bending moduli. This reduction was more pronounced for talin and cortexillin I mutants than for the cortexillin II mutant. The adhesion energy of cells lacking talin was reduced to one-fourth, whereas it was barely impaired in cells deficient in one of the bundling proteins. These results underline an important role of talin in lipid bilayer-cytoskeleton coupling, and indicate a strong influence of this coupling on cell-to-substrate adhesion.

MATERIALS AND METHODS

Culture and preparation of cells

Mutant and wild-type AX2 cells of *Dictyostelium discoideum* were cultivated on SM agar plates, using *Klebsiella aerogenes* as a bacterial food source (Sussmann, 1966). Three different mutants obtained by gene disruption were examined in this study. Mutant HG1666 failed to produce talin (Niewöhner et al., 1997). The two other mutants were defective in the production of either cortexillin I or cortexillin II (Faix et al., 1996). Immediately before the experiment, cells were taken from the edge of a colony and washed three times in cold 17 mM K-Na phosphate buffer (Soerensen), pH 6.0, to remove the bacteria. The washed cells were diluted to a density of $\sim 10^3$ ml^{-1}, injected into the assembled flow chamber, and allowed to attach to the substratum. For all experiments we used a bovine serum albumin (3 mg/ml BSA; Sigma)-coated glass coverslip (60 × 24 × 0.17 mm) as a substratum, which formed the bottom wall of the flow channel. Cells were used for no more than 2 h after injection into the flow chamber.

Setup

The flow chamber consisted of two Plexiglas blocks serving as cover (I) and base plate (II) and of a glass coverslip (Fig. 1 *A*). The coverslip forming the bottom wall of the flow channel was fastened between the base and the cover plate. A rectangular cut across the cover plate served as the actual flow channel. The chamber was sealed with silicon grease and mounted on the stage of an inverted microscope. To allow a laminar flow to become established in the flow chamber, the channel length l has to be greater than ghR_e (Van Kooten et al., 1992). Here, $R_e = \rho Q/(b + h)\eta$ is the Reynolds number; h and b are the channel height and width, respectively; Q is the flow rate in ml/s; ρ and η denote the density and viscosity of the fluid; and g is a numeric factor of $\sim$1.8 (Bowen, 1985). A self-built syringe pump (Fig. 1 *B*) was used for controlling flow rate Q and the resulting shear stress $\sigma = 6\eta Q/bh^2$, ranging from 4 to 12 dyne/cm^2.

For RICM we used an Axiomat inverted microscope (Zeiss, Oberkochen, Germany) with a Zeiss Antiflex-Neofluar 63×/1.25 oil immersion objective, supplemented by nonstandard optical devices for additional magnification. For illumination, the 546.1-nm line of a high-pressure mercury arc lamp (HBO100/W2, Osram) was filtered out with a band-pass filter (line width 5 nm, peak transmission 85%) and reflected by a 50% mirror into the objective. The interference images of adhering cells were projected onto a CCD camera (HR-480; Aqua-TV, Kempten, Germany) and recorded with a 1/4-inch S-VHS video recorder (AG7350; Panasonic). Recorded sequences were digitized with a Macintosh Quadra 950 (Apple Computer) equipped with Pixel Tools imaging boards (Perceptics, Knoxville, TN) and Image VDM software (Perceptics). A customized version of the image analysis software National Institutes of Health-Image (W. Rasband, National Institutes of Health, Bethesda, MD) was used to analyze the interference images.

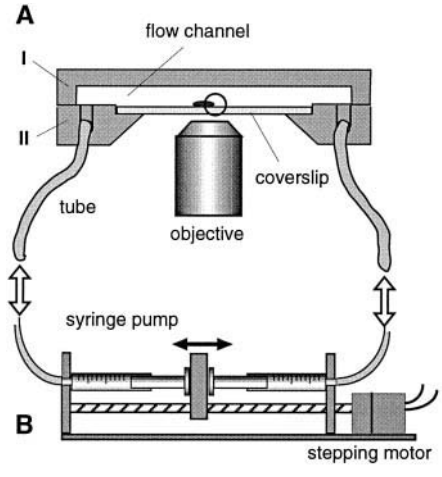

FIGURE 1 Parallel-plate chamber for the measurement of flow-induced deformation of adhering cells. (*A*) Cross section of the flow chamber, consisting of two Plexiglas blocks connected with screws, one block serving as a cover plate (I), the other as a base plate (II). A glass coverslip forming the bottom wall of the flow channel was held in the recess of the base plate. The rectangular flow channel had been cut into the cover plate. The flow channel was 5.9 cm long, 5 mm wide, and 500 μm high. The chamber was sealed with silicon grease. Different flow directions are indicated by the arrows. The encircled area at the edge of a cell adhering to the coverslip denotes the region of interest, which is observed by RICM. (*B*) A home-made syringe pump, consisting of a stepping motor driving two glass syringes, was used for controlling the rate and direction of flow in the channel.

Reconstruction of the cell contour near the contact zone with RICM and digital image processing

We examined the cell contour of adhering cells in terms of the spacing $h(x)$ between cell membrane and substratum, in the proximity of their contact zone, using RICM. The principle of image formation (Gingell and Todd, 1979; Gingell et al., 1982; Rädler and Sackmann, 1992; Kühner and Sackmann, 1996) is illustrated in Fig. 2 *A*. Briefly, light reflected from the substratum (I_1) interferes with light reflected from the ventral cell surface (I_2), giving rise to the following intensity distribution of the image:

$$I(x) = I_1 + I_2 + 2\sqrt{I_1 I_2}\cdot F[\alpha, h(x)] \cdot \cos(2kh(x)\cdot(1 - G(\alpha)) + \delta) \quad (1)$$

Both F and G are functions of the angle α of the illumination aperture, and $k = 2\pi\eta/\lambda$ denotes the wave vector of the illuminating light in the buffer. Assuming that the refractive index of the cell membrane is higher than the index of the surrounding buffer, light reflected on the buffer-cell interface experiences a phase jump of $\delta = \pi$. Therefore, the contact area of an adhering cell appears dark in RICM. Around the adhesion area, interference produces a specific fringe pattern (Fig. 2 *B*) that depends on the shape of the cell contour $h(x)$.

Light reflected from cell organelles in close proximity to the substratum can strongly perturb the interference pattern. These disturbances are recognized by changing the illumination numerical aperture (INA) (Verschueren, 1985; Schindl et al., 1995). To reduce the noise introduced by rapidly moving cell organelles, we usually averaged images over two to five frames. The cell contour was always reconstructed around the edge of the adhesion area, where the distance of the cell wall from the substrate rises continuously with increasing distance from the contact line L (Fig. 2). As has been pointed out in the framework of the "finite-aperture theory" (Rädler and Sackmann, 1993; Gingell and Todd, 1979) or the "nonlocal theory" (Kühner and Sackmann, 1996), the nonzero aperture angle of illumination is important for measurement of the absolute height of an object above the substratum. In the present work only the shape of the cell contour is relevant; the absolute height, however, is not. In this case it is sufficiently accurate to assume a zero aperture angle for calculating $h(x)$, as shown by Kühner et al. (Kühner and Sackmann, 1996). In this simplified approach, an inverse cosine transformation of the observed intensity distribution yields the cell contour $h(x)$:

$$h(x) = \frac{\lambda}{4\pi n}\arccos(I(x) - I_1 - I_2) \quad (2)$$

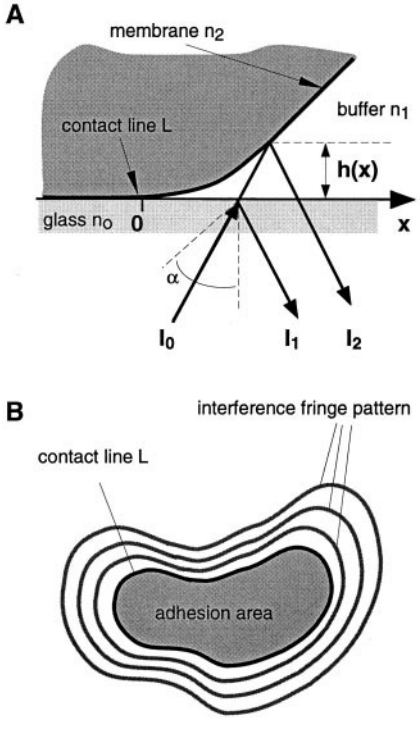

FIGURE 2 Principle of reflection interference contrast microscopy. (*A*) RICM images are formed by interference of light reflected from the surface of the glass substratum (I_1) with light reflected from the cell surface (I_2). The maximum distance $h(x)$ between substratum and cell surface still leading to visible interference fringes decreases with increasing angle α of illumination. For the setup used, this maximum distance was ~1 μm. (*B*) The schematic RICM image of an adhering cell reveals that the adhesion area of a cell appears dark, because of a phase jump of light reflected at the buffer-cell interface. The contact line L circumscribes the adhesion area, where the cell forms close contact with the substratum. Outside of this area, the increasing distance between cell and substratum gives rise to a series of interference fringes.

Elastic model of the cell contour near the substrate

In contrast to the behavior of droplets of partially wetting liquids on solids, the adhesion of soft and closed shells is not only determined by the adhesion energy W and the surface tension γ, but also by the elasticity of the shell. For fluid lipid vesicles only bending elasticity is important, and a rigorous theory relating the shape of the adhering vesicle to the membrane tension, the osmotic pressure, and the adhesion energy is available (Seifert and Lipowsky, 1990). In this case, bending modulus, adhesion energy, and membrane tension can, in principle, be measured by analyzing the three-dimensional shape of the vesicle.

The situation is much more complex for cells, because the cortical shell of a cell is not isotropic and the membrane exhibits bending elasticity as well as shear elasticity. The effect of the latter on the cell shape can be neglected if the adhesion is weak and does not result in area changes of the shell. Recent studies of vesicle adhesion showed that the shape of adhering soft shells near the substrate is determined by the following two boundary conditions: first, the balance of tensions that can be expressed in terms of Young's law,

$$W = \gamma(1 - \cos\vartheta_c) \quad (3a)$$

where ϑ_c is the contact angle and γ is the surface tension; second, the equilibrium of bending moments relating the local radius of curvature $R_c^{-1} = \partial^2 h(x)/\partial x^2$ at the contact line to the bending modulus κ and the adhesion energy W, according to

$$W = \frac{1}{2}\kappa/R_c^2 \quad (3b)$$

Unfortunately, a direct measurement of R_c is difficult and does not yield reliable results (Rädler et al., 1995). Following Bruinsma (1995), the difficulty can be overcome by calculating the approximate contour by minimizing the total free energy ΔG_r of the shell in the rim region around the contact line L. In the absence of strong pinning centers, the contact line does not exhibit sharp edges. In this case the above boundary conditions must be fulfilled locally, and the free energy ΔG of the contour per unit length is

$$\Delta G = \int_0^\infty \left\{\frac{\kappa}{2}\left(\frac{\partial^2 h(x)}{\partial x^2}\right) + \frac{\kappa}{2}\left(\frac{\partial h}{\partial x}\right)^2\right\}dx - \int_{-\infty}^0 W(x)\mathrm{d}x \quad (4)$$

Minimizing ΔG yields a fourth-order differential equation,

$$\gamma\frac{\partial^2 h}{\partial x^2} - \kappa\frac{\partial^4 h}{\partial x^4} = 0 \quad (5)$$

The characteristic length scale $\lambda = \sqrt{\kappa/\gamma}$ embedded in this differential equation separates regions of the cell contour dominated by lateral tension from regions near the contact line that are dominated by the bending modulus (Fig. 3). The above description of the cell contour does not apply to regions of the cell where the membrane curvature within the plane of the substratum becomes large compared to the curvature perpendicular to the substratum (or $1/\lambda$). In particular, this is the case in close proximity to strong pinning centers, where sharp edges at the contact line would be associated with an infinitely small bending energy. Therefore, measurements were not performed in the vicinity of pinning centers.

A solution $h(x)$ of Eq. 5 can be obtained by considering the following boundary conditions: $h(x) = 0$ within the contact area and $h(x) = \vartheta_c x$ for x large and positive (Fig. 3), where ϑ_c denotes the macroscopic contact angle (Bruinsma, 1996):

$$h(x) = \begin{cases} \vartheta_c(x - \lambda) + \vartheta_c\lambda e^{-x/\lambda} & x \geq 0 \\ 0 & x < 0 \end{cases} \qquad (6)$$

The contact angle ϑ_c can be directly measured by a least-squares fit to the tension-dominated linear part of the reconstructed cell contour (Fig. 3). The distance between the contact line and the intersection of the linear fit with the x axis defines the characteristic length λ. Note that the contact line is usually well defined by a sharp increase in the intensity of the RICM image at the edge of the adhesion area, as in the example in Fig. 5 *C*.

RESULTS

Effect of small shear forces on the cell contour

As outlined in Materials and Methods, analysis of the contact contour yields only two parameters, λ and ϑ_c, whereas we have three unknown parameters (γ, κ, and W). To obtain absolute values of bending stiffness κ and membrane tension γ, we studied the effects of small shear forces on the contour and the length scale λ, using wild-type and mutant cells of *Dictyostelium discoideum*. The shear stresses applied ranged from 4 to 12 dyne/cm^2. They were small enough to prevent strong deformation or detachment of the cells, as checked by phase-contrast microscopy. Yet these shear stresses were large enough to measurably alter the contact angle and contact curvature of the cell.

The relationship between shear flow and the resulting shape of adhering cells is very complicated and has only been solved numerically for a few spherically symmetrical cell geometries (Goldmann et al., 1967; Olivier and Truskey, 1993). For the analysis of nonsymmetrical cells, as examined in the present work, we concentrated on the effect of shear forces at the boundary region between cell surface and substrate, adopting the following approximation. Because of the bending stiffness of the composite membrane, the shear force acting on the dorsal cell surface changes the tension at the contact line (Bruinsma, 1995). According to a theorem of shell elasticity (Landau and Lifschitz, 1989), the resultant of the load above the surface must be compensated by a shift in the tension of the shell at the surface in the direction of the load. Therefore, the tension increases by $\Delta\gamma$ at the edge of the cell facing the flow and decreases at the opposite side by the same amount (Fig. 4). We used laser scanning microscopy to determine the average height of wild-type cells. To facilitate comparison of wild-type and mutant cells, we evaluated only cells that had approximately the same size (controlled by bright-field microscopy) and exhibited adhesion areas of comparable size (controlled by RICM), so that the height of all cells could be considered to be in the same range of $\sim$5 μm. This height was small compared to the typical dimension of a cells contact area of $\sim$15 μm, or the height of the flow channel of 500 μm. Considering this flat cross section of the cells along the direction of flow, the load on the cell can be approximated by σL_o, where σ is the applied shear stress and L_o denotes the width of the contact area parallel to the direction of flow.

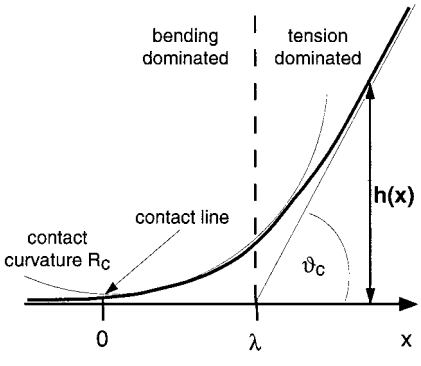

FIGURE 3 Theoretical height profile of adhering soft shells near the contact area. The predicted height profile $h(x)$ perpendicular to the contact line is governed by two boundary conditions, the balance of tensions and the equilibrium of bending moments. The characteristic length λ separates two regimes. For distances $x < \lambda$ the cell contour is dominated by the bending energy and is therefore curved. For $x > \lambda$ the contour is dominated by the lateral tension of the composite membrane, and approaches a straight line. Extrapolation of this line to the substratum defines both λ and the contact angle ϑ_c.

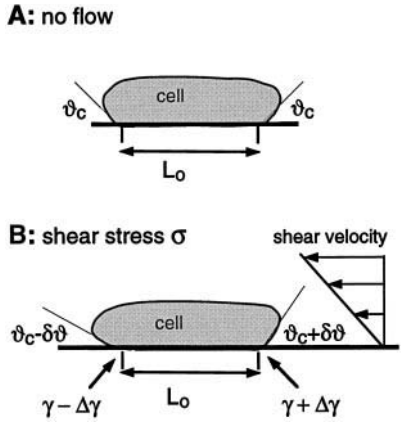

FIGURE 4 Deformation of a cell in response to shear. (*A*) A schematic cross section of an undisturbed adhering cell exhibiting the contact angle ϑ_c with the substratum. If the cell is exposed to a laminar shear flow (*B*), the contact angle is measurably increased on the edge of the cell facing the flow and is decreased on the opposite side. This change in contact angles is accompanied by a shift in membrane tension γ due to the shear stress exerted on the cell. For flat cells the shear stress σ results in an increase in the lateral tension at the edge facing the flow by approximately $\Delta\gamma \approx \sigma L_o/2$ and a decrease at the opposite side by the same amount. Note that for the weak deformations used in this study, the diameter of the adhesion area L_o does not significantly change because of the flow.

Therefore, the flow-induced increase in tension $\Delta\gamma$ at the edge of the cell facing the flow is given by

$$\Delta\gamma \approx \frac{1}{2}\sigma L_o \tag{7}$$

Note that this equation only holds for small deformations, where the bending modulus of the shell remains unaffected. The shear-induced change in tension $\Delta\gamma$ will therefore change the characteristic length λ in a predictable way. By measuring λ in the absence of flow ($\lambda = \sqrt{\kappa/\gamma}$) and in the presence of flow ($\lambda = \sqrt{\kappa/(\gamma + \Delta\gamma)}$), we have two equations, from which both membrane tension γ and the bending modulus κ can be obtained. The adhesion energy W can be derived from Young's law (Eq. 3a) by measuring the contact angle in the stress-free state.

The height profile of an undisturbed cell was reconstructed from RICM images along a section perpendicular to the contact line L. The characteristic length λ and the contact angle ϑ_c were obtained from a least-squares fit to the linear portion of the profile. Subsequently, the same measurement was repeated along the same section shortly after a shear force was applied (Fig. 5). Note that the length-scale λ decreases under the influence of flow, as predicted. Cell contours were always reconstructed at the side of the cell facing the direction of flow. To avoid artifacts due to changes in the fringe pattern caused by active cell movement, the time interval between measurements of the two compared contours was always <0.5 s. Furthermore, we chose only cells that exhibited a straight edge approximately perpendicular to the direction of flow, which did not change considerably during this short time interval. Measurements were not performed in the vicinity of pinning centers, where additional strong lateral tensions mask the effect of the applied flow. Finally, the cell density in the flow channel (10^3 ml^{-1}) was sufficiently small to prevent neighboring cells from affecting the laminar flow profile in the vicinity of an examined cell.

Influence of three actin-binding proteins on membrane tension, bending modulus, and adhesion energy

Values for the contact angle α and the characteristic length λ of wild-type and mutant cells were determined and used for the calculation of membrane tension γ, bending stiffness κ, and adhesion energy W. To facilitate a comparison of the results, only cells with approximately equal volume and height were evaluated.

In the absence of an external force, wild-type and mutant cells exhibited almost identical contact angles of $\sim$22°. Remarkable differences were observed, however, in the presence of flow. In Fig. 6 histograms of the bending moduli, adhesion energies, and lateral tensions are shown for all types of cells examined. As typical for measurements on single living cells, the distributions were broad. Nevertheless, the differences between wild-type and mutant cells could be clearly established. The bending modulus κ was strongly reduced for cells deficient in cortexillin I, and even more for talin-deficient cells. Removal of cortexillin II produced a smaller but still obvious reduction of κ.

A remarkable difference between cortexillin I and II mutants on one side and the talin mutant on the other was observed in their lateral membrane tensions γ and their adhesion energies W. In talin-deficient cells, W and γ were markedly reduced, similar to the bending energy κ. In contrast, only a slight reduction in W and γ was observed for cells lacking cortexillin I. No reduction in these two parameters could be observed for cells deficient in cortexillin II. Table 1 summarizes the results obtained for wild-type and mutant cells lacking cortexillin I, cortexillin II, or talin.

DISCUSSION

Elastic properties deduced from local measurements of adhering cells

To assess the influence of actin-binding proteins on the elastic properties of motile cells, we developed an interferometric technique to evaluate small local deformations of adhering cells that are caused by hydrodynamic shear forces. These deformations of the cell contour close to the substratum can be analyzed in terms of two simple boundary conditions, the balance of tensions and the equilibrium of bending moments, without having to consider the complex shape of the cell as a whole. By applying this technique to wild-type and mutant cells of *Dictyostelium discoideum,* a marked dependence of the bending modulus κ and the adhesion energy W on both the rigidity of the cytoskeleton and its coupling to the lipid-protein bilayer was observed. Our results, quantifying changes in the physical properties of cells that are caused by the absence of certain cytoskeletal proteins, can be interpreted in the framework of the minimum elastic energy concept (Seifert and Lipowsky, 1990; Schindl et al., 1995; Bruinsma, 1995).

The length scale in our experiments of $\sim$1 μm is too large for seeing small-scale heterogeneities in the actin cortex. However, there may be more global differences in the membrane properties, for instance, between the leading and trailing edges of the cell. To make measurements between different strains comparable, we have therefore always performed measurements on the side of the cell.

Effect of cytoskeletal proteins on the bending modulus

The bending modulus κ was significantly decreased in mutant cells deficient in talin or either isoform of cortexillin, as compared to wild-type cells (Table 1, Fig. 6). The reduction was most pronounced for cells lacking talin, where we determined a value of κ comparable to that of a phosopholipid vesicle containing $\sim$50% cholesterol (Sackmann, 1995). This finding underlines the important role of talin, a protein implicated in coupling of the cytoskeleton to

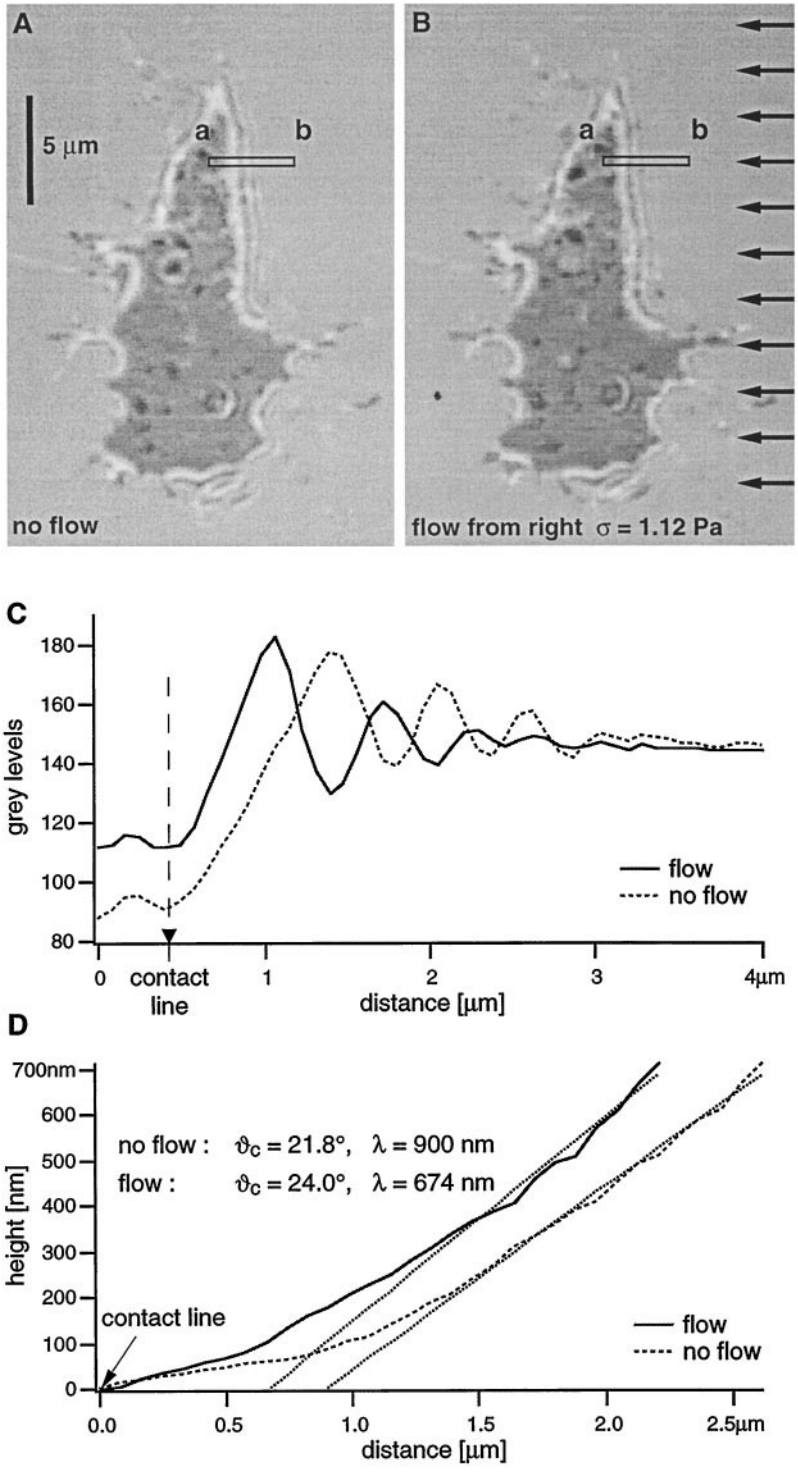

FIGURE 5 RICM images, fringe patterns, and contact angles in the absence and presence of shear. To exemplify the experimental data, typical RICM images are shown of a wild-type *Dictyostelium discoideum* cell adhering to albumin-coated glass in the absence (*A*) or the presence (*B*) of a laminar flow. Darker and brighter patches visible within the adhesion area are caused by intracellular compartments such as vacuoles and mitochondria. The time interval between two images is <0.5 s. In *C* the intensity distributions along the line from *a* to *b* are shown, as marked in *A* (– – –) and *B* (——). From this distribution the cell contour is reconstructed as described in Materials and Methods. The sharp increase in intensity of the RICM images at the edge of the adhesion area defines the location of the contact line. As seen in *D*, the profile in the presence of flow (——) exhibits a smaller value of λ (674 nm) than the profile in the absence of flow (– – –, $\lambda = 900$ nm), in agreement with the theory.

the lipid-protein bilayer in vertebrate cells (for reviews see Geiger et al., 1995; Jockusch et al., 1995).

Cortexillin is known to bundle actin filaments and to connect these bundles into meshworks (Faix et al., 1996). The elimination of cortexillin I by gene disruption resulted in a stronger impairment of cell division than the elimination of cortexillin II (Faix et al., 1996). In agreement with these findings, the reduction of bending moduli was significantly stronger for cells lacking cortexillin I than for cells lacking cortexillin II. Cells of the double mutant lacking both cortexillins I and II were extremely flat and, because of a dramatic impairment of cell division, very large. These cells proved to be inappropriate for the measurements performed in the present study.

Our results can be related to data obtained in cell populations by the use of a torsional rheometer. Measurements

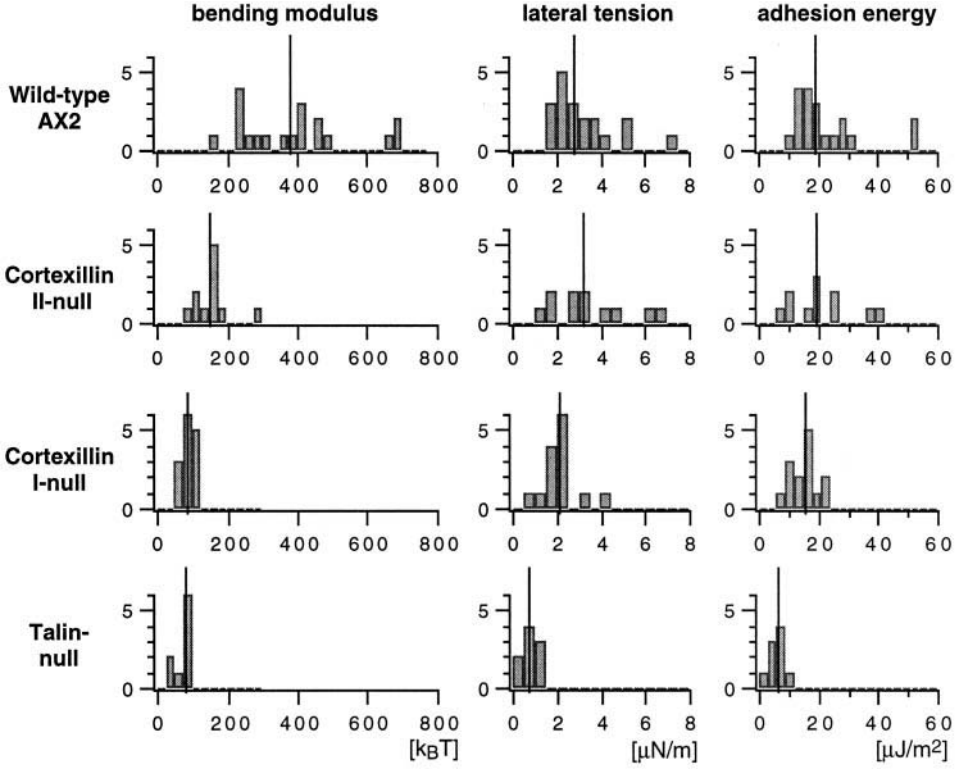

FIGURE 6 Histograms of membrane bending moduli, lateral tensions, and adhesion energies determined for wild-type and mutant cells of *Dictyostelium discoideum*. In each histogram, the y axis denotes the number of cells. The mutants compared with wild-type AX2 were deficient in cortexillin II, cortexillin I, or talin. Medians of the distributions are denoted by a vertical line. Numbers of cells analyzed were 19 (AX2), 11 (cortexillin II-null), 14 (cortexillin I-null), or 9 (talin-null). The distributions of membrane tensions and adhesion energies obtained for cortexillin I mutants differ significantly from the results for AX2 cells. The Mann-Whitney U-test revealed a probability of $p < 0.01$ that these distributions would be identical.

showed a markedly decreased shear modulus μ in mutants that lack the two F-actin cross-linking proteins α-actinin and 120-kDa gelation factor (Eichinger et al., 1996). For isotropic systems, the shear modulus μ can be expressed in terms of the Young's modulus E by $\mu = E/(2 + \sigma)$, which in turn is related to the bending modulus κ by $\kappa = Eh^3/12(1 - \sigma^2)$ (Landau and Lifschitz, 1989). Here h is the thickness of the cell cortex and σ is the Poisson ratio, which is ~0.5. Although this relationship between μ and κ holds only approximately for cells, a reduction in μ also suggests a decrease in the bending modulus κ of the cell cortex.

Lowered adhesion energy in cells lacking cytoskeletal proteins

Key parameters for the bending modulus and the lateral tension of the composite membrane are both the intrinsic rigidity of the actin cortex and its coupling to the lipid-protein bilayer. As known from a variety of studies in vitro, the rigidity of the actin cortex is determined by a large number of actin-binding proteins mediating cross-linkage and bundling of actin filaments (Sato et al., 1987; Janmey et al., 1990).

Lateral tension and bending energy of the cell envelope have, in fact, a strong bearing on the adhesion of a cell. As known from erythrocyte studies (Zilker et al., 1992), cell membranes exhibit thermally induced undulations, leading to repulsive forces. These undulation forces, as discussed by Seifert and Lipowsky (1990), have been shown experimentally to substantially reduce the van der Waals attraction and thus the adhesion energy (Rädler et al., 1995). Reduction of lateral tension γ or bending modulus κ of the composite membrane increases the undulations and therefore leads to a smaller adhesion energy. Because κ and γ are significantly smaller for the lipid-protein bilayer alone, as compared to the composite cell membrane, disruption of the bilayer-cortex coupling can be expected to result in a pronounced reduction of the adhesion energy.

TABLE 1 Comparison of effective contact angle, membrane bending modulus, membrane tension, and cell adhesion energy on albumin-covered glass for cells of the wild type (AX2) and the mutants indicated

	AX2 (19)	Talin-null (9)	Cortexillin I-null (14)	Cortexillin II-null (11)
Contact angle* (°)	21.5 ± 1.8	21.8 ± 1.9	22.3 ± 1.8	20.5 ± 2.2
Bending modulus (k_BT)	391 ± 156	71 ± 21	94 ± 18	159 ± 51
Membrane tension (μN/m)	3.1 ± 1.4	0.8 ± 0.3	2.2 ± 0.8	3.5 ± 1.8
Adhesion energy (10^{-6} J/m^2)	22.0 ± 12.2	5.9 ± 2.4	15.2 ± 4.7	21.2 ± 10.0

*The effective contact angle was measured at zero shear stress. Means are shown with their standard deviations. The numbers in parentheses denote the number of cells examined for each wild-type or mutant strain.

In previous work it was shown that the locomotion of *Dictyostelium* cells deficient in the three actin-binding proteins α-actinin, 120-kDa gelation factor, and severin was not significantly affected on strongly adhesive substrates such as albumin-covered glass (Schindl et al., 1995; Weber et al., 1995). In contrast, the motility of the mutant cells was strongly impeded on weak adhesive substrates such as freshly cleaved mica. The differences in motility were tentatively attributed to a substantial reduction of the adhesion strength of these mutants, due to a smaller bending modulus of the bilayer-cytoskeleton composite membrane. This hypothesis was based on theoretical considerations showing that both the shape and the state of adhesion of vesicles or cells are determined by the minimum of the total free elastic energy (Seifert and Lipowsky, 1990; Bruinsma, 1995).

Our results, demonstrating that cortexillins and talin influence the adhesion energy to different degrees, provide strong evidence that undulation forces can substantially decrease the adhesion energy of cells, if the coupling between the lipid-protein bilayer and the actin cortex is weak. Whereas the lack of cortexillin II had no significant effect, and the removal of cortexillin I had only a moderate influence, the lack of talin markedly reduced adhesion of the cell to albumin-covered glass (Fig. 6, Table 1). This strong decrease in the adhesion energy of the talin mutant also substantiates biological studies indicating that talin is involved not only in the adhesion of *Dictyostelium* cells to a substrate on which they move, but also in adhesion to particles to be phagocytosed, and in adhesion of the cells to each other (Niewöhner et al., 1997).

It is well established that in fibroblasts or platelets, talin plays a key role in the coupling of the cytoskeleton to the lipid protein-bilayer through integrins (Isenberg and Goldmann, 1992; Nuckolls et al., 1992; Albigès-Rizo et al., 1995). Our results suggest that in *Dictyostelium* too, talin binds to a transmembrane protein. The pronounced reduction of membrane bending modulus κ and lateral tension γ in talin-null mutants provides evidence for this role of talin in coupling. Elimination of talin may therefore directly affect a specific protein-mediated interaction between the actin cortex and the plasma membrane. The bending modulus we determined for talin-deficient cells was comparable to that of a phospholipid vesicle containing 50% cholesterol (Sackmann, 1995). The plasma membrane of *Dictyostelium* contains ~20% cholesterol (Weeks and Herring, 1980). Thus the bending modulus of its lipid bilayer alone should be still lower than the measured one. Nevertheless, the low value of κ obtained for the talin-null mutant indicates a strong effect of talin relative to ponticulin (Hitt et al., 1994; Shutt et al., 1995), hisactophilin (Scheel et al., 1989; Behrisch et al., 1995; Hanakam et al., 1996), or other potential coupling proteins.

We thank Dr. Robin Bruinsma for helpful discussions.

This work was supported by the Deutsche Forschungsgemeinschaft (SFB 266).

REFERENCES

Albigès-Rizo, C., P. Frachet, and M. R. Block. 1995. Down regulation of talin alters cell adhesion and the processing of the $\alpha 5\beta 1$ integrin. *J. Cell Sci.* 108:3317–3329.

Alon, R., D. A. Hammer, and T. A. Springer. 1995. Lifetime of the P-selectin carbohydrate bond and its response to tensile force in hydrodynamic flow. *Nature.* 374:539–542.

Behrisch, A., C. Dietrich, A. A. Noegel, M. Schleicher, and E. Sackmann. 1995. The actin-binding protein hisactophilin binds in vitro to partially charged membranes and mediates actin coupling to membranes. *Biochemistry.* 34:15182–15190.

Bowen, B. D. 1985. Streaming potential in the hydrodynamic entrance region of cylindrical and rectangular capillaries. *J. Colloid Interface Sci.* 106:367–376.

Bruinsma, R. 1995. Adhesion and rolling of leukocytes: a physical model. *Proc. NATO Adv. Inst. Phys. Biomater. NATO ASI Ser.* 332:61–75.

Eichinger, L., B. Köppel, A. A. Noegel, M. Schleicher, M. Schliwa, K. Weijer, W. Witke, and P. A. Janmey. 1996. Mechanical perturbation elicits a phenotypic difference between *Dictyostelium* wild-type cells and cytoskeletal mutants. *Biophys. J.* 70:1054–1060.

Evans, E. A. 1985. Detailed mechanics of membrane-membrane adhesion and separation. I. Continuum of molecular cross bridges. *Biophys. J.* 48:175–183.

Faix, J., M. Steinmetz, H. Boves, R. A. Kammerer, F. Lottspeich, U. Mintert, J. Murphy, A. Stock, U. Aebi, and G. Gerisch. 1996. Cortexillins, major determinant of cell shape and size, are actin bundling proteins with a parallel coiled-coil tail. *Cell.* 86:631–642.

Gallik, S., S. Usami, K. M. Jan, and S. Chien. 1989. Shear stress-induced detachment of human polymorphonuclear leukocytes from endothelial cell monolayers. *Biorheology.* 26:823–834.

Geiger, B., S. Yehuda-Levenberg, and A. D. Bershadsky. 1995. Molecular interactions in the submembrane plaque of cell-cell and cell-matrix adhesions. *Acta Anat.* 154:46–62.

Gingell, D., and I. Todd. 1979. Interference reflection microscopy. A quantitative theory for image interpretation and its application to cell-substratum separation measurements. *Biophys. J.* 26:507–526.

Gingell, D., I. Todd, and O. S. Heavens. 1982. Quantitative interference microscopy: effect of microscope aperture. *Opt. Acta (Lond.).* 29: 901–908.

Goldmann, A. J., R. G. Cox, and H. Brenner. 1967. Slow viscous motion of a sphere parallel to a plane wall. II. Couette flow. *Chem. Eng. Sci.* 22:653–660.

Hammer, D. A., and D. A. Lauffenburger. 1987. A dynamical model for receptor-mediated cell adhesion to surfaces. *Biophys. J.* 52:475–487.

Hanakam, F., G. Gerisch, S. Lotz, T. Alt, and A. Seelig. 1996. Binding of hisactophilin I and II to lipid membranes is controlled by a pH-dependent myristoyl-histidine switch. *Biochemistry.* 35:11036–11044.

Hitt, A. L., J. H. Hartwig, and E. J. Luna. 1994. Ponticulin is the major high affinity link between the plasma membrane and the cortical actin network in *Dictyostelium. J. Cell Biol.* 126:1433–1444.

Horwitz, A., K. Duggan, C. Buck, M. C. Beckerle, and K. Burridge. 1986. Interaction of plasma membrane fibronectin receptor with talin—a transmembrane linkage. *Nature.* 320:531–533.

Isenberg, G., and W. H. Goldmann. 1992. Actin-membrane coupling: a role for talin. *J. Muscle Res. Cell Motil.* 13:587–589.

Janmey, P. A., S. Hvidt, J. Lamb, and T. P. Stossel. 1990. Resemblance of actin binding protein/actin gels to covalently crosslinked networks. *Nature.* 345:89–92.

Jockusch, B. M., P. Bubeck, K. Giehl, M. Kroemker, J. Moschner, M. Rothkegel, M. Rüdiger, K. Schlüter, G. Stanke, and J. Winkler. 1995. The molecular architecture of focal adhesions. *Annu. Rev. Cell Dev. Biol.* 11:379–416.

Kaufmann, S., J. Käs, W. H. Goldmann, E. Sackmann, and G. Isenberg. 1992. Talin anchors and nucleates actin filaments at lipid membranes. *FEBS Lett.* 314:203–205.

Kühner, M., and E. Sackmann. 1996. Ultrathin hydrated dextran films grafted on glass: preparation and characterization of structural, viscous and elastic properties by quantitative microinterferometry. *Langmuir.* 12:4866–4876.

Landau, L. D., and E. M. Lifschitz. 1989. Theory of Elasticity, 6th Ed. Akademie Verlag, Berlin.

Lipowsky, R., and E. Sackmann. 1995. Structure and Dynamics of Membranes. Elsevier, Amsterdam.

Niewöhner, J., I. Weber, M. Maniak, A. Müller-Taubenberger, and G. Gerisch. 1997. Talin-null cells of *Dictyostelium* are strongly defective in adhesion to particle and substrate surfaces and slightly impaired in cytokinesis. *J. Cell Biol.* 138:349–361.

Nuckolls, G. H., L. H. Romer, and K. Burridge. 1992. Microinjection of antibodies against talin inhibits the spreading and migration of fibroblasts. *J. Cell Sci.* 102:753–762.

Olivier, L. A., and G. A. Truskey. 1993. A numerical analysis of force exerted by laminar flow on spreading cells in a parallel plate flow chamber assay. *Biotechnol. Bioeng.* 42:963–973.

Rädler, J., T. J. Feder, H. H. Strey, and E. Sackmann. 1995. Fluctuation analysis of tension-controlled undulation forces between giant vesicles and solid substrates. *Phys. Rev. E.* 51:4526–4536.

Rädler, J., and E. Sackmann. 1992. On the measurement of weak repulsive and frictional colloidal forces by reflection interference contrast microscopy. *Langmuir.* 8:848–853.

Rädler, J., and E. Sackmann. 1993. Imaging optical thicknesses and separation distances of phospholipid vesicles at solid surfaces. *J. Phys. II France.* 3:727–748.

Sackmann, E. 1994. Intra- and extracellular macromolecular networks: physics and biological function. *Macromol. Chem. Phys.* 195:7–28.

Sackmann, E. 1995. Physical basis of self-organization and function of membranes: physics of vesicles. *In* Structure and Dynamics of Membranes, Vol. 1A. R. Lipowsky and E. Sackmann, editors. Elsevier/North Holland, Amsterdam. 213–304.

Sato, M., W. H. Schwarz, and T. D. Pollard. 1987. Dependence of the mechanical properties of actin/α-actinin gels on deformation rate. *Nature.* 325:828–830.

Scheel, J., K. Ziegelbauer, T. Kupke, B. M. Humbel, A. A. Noegel, G. Gerisch, and M. Schleicher. 1989. Hisactophilin, a histidin-rich actin-binding protein from *Dictyostelium discoideum. J. Biol. Chem*. 264: 2832–2839.

Schindl, M., E. Wallraff, B. Deubzer, W. Witke, G. Gerisch, and E. Sackmann. 1995. Cell-substrate interactions and locomotion of dictyostelium wild-type and mutants defective in three cytoskeletal proteins: a study using quantitative reflection interference contrast microscopy. *Biophys. J.* 68:1177–1190.

Seifert, U., and R. Lipowsky. 1990. Adhesion of vesicles. *Phys. Rev. A.* 42:4768–4771.

Shutt, D. C., D. Wessels, K. Wagenknecht, A. Chandrasekhar, A. L. Hitt, E. J. Luna, and D. R. Soll. 1995. Ponticulin plays a role in the positional stabilization of pseudopods. *J. Cell Biol.* 131:1495–1506.

Sussmann, M. 1966. Biochemical and genetic methods in the study of cellular slime mold development. *Methods Cell Physiol.* 2:397–410.

Tissot, O., A. Pierres, C. Foa, M. Delaage, and P. Bongard. 1992. Motion of cells sedimenting on a solid surface in laminar shear flow. *Biophys. J.* 61:204–215.

Van Kooten, T. G., J. M. Schakenraad, H. C. Van der Mei, and H. J. Busscher. 1992. Development and use of a parallel-plate flow chamber for studying cellular adhesion to solid surfaces. *J. Biomed. Mater. Res.* 26:725–738.

Verschueren, H. 1985. Interference reflection microscopy in cell biology: methodology and applications. *J. Cell Sci.* 75:279–301.

Weber, I., E. Wallraff, R. Albrecht, and G. Gerisch. 1995. Motility and substratum adhesion of *Dictyostelium* wild-type and cytoskeletal mutant cells: a study by RICM/bright-field double view image analysis. *J. Cell Sci.* 108:1519–1530.

Weeks, G., and F. G. Herring. 1980. The lipid composition and membrane fluidity of *Dictyostelium discoideum* plasma membranes at various stages during differentiation. *J. Lipid. Res.* 21:681–686.

Xia, Z., H. L. Goldsmith, and T. G. M. van de Ven. 1993. Kinetics of specific and nonspecific adhesion of red blood cells on glass. *Biophys. J.* 65:1073–1083.

Xia, Z., H. L. Goldsmith, and T. G. M. van de Ven. 1994. Flow induced detachment of red blood cells adhering to surfaces by specific antigen-antibody bonds. *Biophys. J.* 66:1222–1230.

Xiao, Y., and G. A. Truskey. 1996. Effect of receptor-ligand affinity on the strength of endothelial cell adhesion. *Biophys. J.* 71:2869–2884.

Zhao, Y., S. Chien, and R. Skalak. 1995. A stochastic model of leukocyte rolling. *Biophys. J.* 69:1309–1320.

Zilker, A., M. Ziegler, and E. Sackmann. 1992. Spectral analysis of erythrocyte flickering in the 0.3–4 μm^{-1} regime by microinterferometry combined with fast image processing. *Phys. Rev. A.* 46:7998–8001.